Numerical investigation of the effect of confined curved waterways on ship hydrodynamics

Bo Yang[1,2,*], Emmanuel Lefrançois[1], Sami Kaidi[2]

[1] Laboratoire Roberval, Sorbonne université, Université de technologie de Compiègne, 60203 Compiègne cedex, France. E-mail: bo.yang@utc.fr, web: https://www.utc.fr

[2] CEREMA-DtecREM (Center for Studies and Expertise on Risks, the Environment, Mobility and Urban Planning), 60280 Margny-lès-Compiègne, France. Email: sami.kaidi@cerema.fr, web: https://www.cerema.fr

[*] Corresponding author: Bo Yang, bo.yang@utc.fr

ABSTRACT

Inland ships are susceptible to accidents in confined curved waterways. Considering the inadequate research till now, this paper investigates and analyzes the influence of channel angle, water depth to draft ratio, and ship speed on ship hydrodynamics in confined curved channels utilizing the CFD method. To simulate the flow around a three-dimensional ship model, the unsteady Navier-Stokes equations that are enclosed by the realizable K-Epsilon turbulence model are used. Mesh verification analysis is performed to choose the most acceptable grid dimension, and then the CFD model is validated in a normal confined channel by comparing the forces of numerical resistance with those from experiments. Finally, nearly 40 numerical simulations considering various parameters are conducted, and their effects on ship hydrodynamics are analyzed in detail.

Keywords: CFD simulations; curved channel; inland navigation; confined waterways; ship hydrodynamics

NOMENCLATURE

$\boldsymbol{V}$ Velocity [m s^{-1}]
V_s Ship speed [m s^{-1}]
p Pressure [Pa]
ρ Fluid density [Pa s]
η Kinematic viscosity [N s m^{-1}]
α Channel angle [°]
h/T Water depth to draft ratio [-]
W Channel bottom width [m]
β Drift angle [°]
L_{pp} Length between perpendiculars [m]
B Beam [m]
H Height [m]
C_b Block coefficient [-]
W_s Wetted surface area of ship [m^2]
C_s Cross area of ship [m^2]
X Resistance force [N]
Y Sway force [N]
N Yaw moment [N]
X' Non-dimensional resistance force [-]
Y' Non-dimensional sway force [-]
N' Non-dimensional yaw moment [-]
R_i Convergence ratio [-]
C_i Correction factor [-]
δ_i Numerical error [-]
P_i Order of accuracy [-]
U_i Uncertainty [-]
E Errors [%]

1. INTRODUCTION

Nowadays, inland waterway transport is playing a more and more significant role thanks to its various advantages over the other transportation modes, such as low cost and low environmental pollution, etc. However, inland rivers are normally narrow with many bending sectors. Ships' navigating in confined curved channels has always been a tough problem to deal with due to the complexity of flow. In such a navigational environment, ships will be faced with not only the confined environment but also the complicated flow characteristics caused by centrifugal force, such as the different water depth between concave and convex side, loop flow. Especially this is coupled with an increasingly larger size of vessels in inland waterways. All of these above increases the risk of accidents for ship navigating. Till now, research on bending scales is insufficient, and there is no unified conclusion about how to set the bending scale safely and effectively.

Even so, many researchers have attempted research work in this area. Some scholars studied the flow characteristics in the bending of rivers. Li et al. (2020) compared and analyzed the flow characteristics of curved rivers with 3 different degrees employing the CFD tool Fluent. Aseperi (2018) investigated the impact of curvature radius and inertial forces on the flow characteristics of an idealistic river bend with the CFD method. Ai and Zhu (2020) developed a measurement equation for drift angle and verified its close relation with a set of parameters like channel radius and water depth, etc. Vujičić et al. (2018) put forward a realistic and analytical approach focused on knowledge and practice to the evaluation of secure maneuvering for ship's turning in confined waterways.

In recent years, CFD is more and more widely used for numerical research and analysis in many regions, including predicting ship hydrodynamics. Experiments not only are costly but also will omit the details of the flow field, while numerical research with CFD both costs less and contributes to our analyzing the mechanisms of flow. Tezdogan et al. (2015) utilized the CFD tool STARCCM+ to predict the squat and resistance of a model container ship under different ship drafts and ship speeds. Their numerical results were highly consistent with experimental ones. After this, they conducted a computational analysis of ship movements in shallow water to model the ship's heave and pitch reactions to head waves (Tezdogan et al., 2016). Subsequently, a parametric comparison of the behavior and efficiency prediction techniques in shallow waters was carried out by Terziev et al. (2018), the key goal of which is to determine how a change in channel topography affects ship sinkage, trim, and resistance.

With the CFD method, Kaidi et al. (2017) numerically investigated the effect of the bank-propeller-hull relationship on ship manoeuvring. After that, they studied the impact of confined waters on force interaction between hull, propeller, and rudders of an inland container ship (Kaidi et al., 2018). Also, he worked with Razgallah looked at how free surface simulation affected ship hydrodynamic forces in inland channels, taking into account varying water depths, ship speeds, and even drift angle(Razgallah et al., 2018). More recently, they checked the capacity of the CFD method for modeling and measuring the impact of mud on the hydrodynamic loads exerted on the vessel (Kaidi et al., 2020). Compared with the results from experiments, their results showed good agreement, which proves the ability of the CFD system to replicate difficult-to-achieve configurations in a towing tank. Also, Bechthold and Kastens (2020) simulated the sinkage and trim of 3 Postpanmax container ships in confined shallow waters by virtue of STARCCM+. Their results displayed reliable uniformity when compared with model test data. To evaluate the relative effects of canal depth and/or width constraints on the overall ship sailing performance, Khaled Elsherbiny et al. (2020) analyzed hydrodynamic phenomena of ships sailing through the Suez Canal in the permitted speed range utilizing STARCCM+. Finally, a clear correlation between the canal's cross-section and all the parameters studied was revealed.

Till now, there is no clear research on the effect of confined curved waterways on ship hydrodynamics.

Considering the high cost and insecurity of real ship experiments, this paper conducts a numerical investigation on the influence of different parameters in curved channels on ship hydrodynamics, including channel angles(α), water depth to draft ratio(h/T), and ship speed(V_s) of the ship. Due to the limited space here, we don't present the effect of channel bottom width(W) and drift angle(β) on ship hydrodynamics, as well as the maneuvering analysis. This paper aims to understand the physical phenomena around the ship regarding different parameters, and then improves the simulators by proposing some mathematical formulations that include these effects.

2. NUMERICAL METHOD

In this study, all the simulations are conducted with the CFD tool STARCCM+. The incompressible viscous flow around the ship is obtained by solving the unsteady Navier-Stokes equations, which are given in equation (1) and (2)(Kaidi et al., 2020):

$$\nabla \cdot \boldsymbol{V} = 0 \tag{1}$$

$$\frac{\partial \boldsymbol{V}}{\partial \mathrm{t}} + \nabla \cdot (\boldsymbol{V} \otimes \boldsymbol{V}) = -\frac{1}{\rho}\nabla p + \frac{\eta}{\rho}\nabla^2 \boldsymbol{V} \tag{2}$$

Where $\boldsymbol{V}$ is velocity; p is pressure; ρ and η are fluid density and kinematic viscosity respectively.

The RANS K-Epsilon turbulence model is used to close the equations above. Also, Volume of Fluid (VOF) method is used to predict the free surface.

3. NUMERICAL MODEL AND SIMULATION CASES

3.1 Numerical Model

The specific characteristics of the ship model in this research are illustrated in Table 1. The real ship is a container ship whose scale factor is 25 times as large as the ship model studied here.

Table 1. Characteristics of the ship model

	Length between perpendiculars, L_{pp}/m	Beam, B/m	Height, H/m	Draft, T/m	Block coefficient, C_b	Wetted surface area of ship, W_s/m^2	Cross area of ship, C_s/m^2
Ship model scale	5.4	0.45	0.24	0.1	0.899	3.367	0.0545

3.2 Numerical Configuration

There are 5 diverse configurations set up here as depicted in Table 2, where the bank slope angle is 27°, and the ship draft is 0.1m. Every configuration focuses on different parameters. Totally, nearly 40 simulations were conducted in this work.

Table 2. Simulation configuration

Config.	Channel angle, α/°	h/T ratio	Ship speed, $V_s/m\ s^{-1}$	Channel bottom width, W/m	Drift angle, β/°	Number of simulations

1	30°,60°, 90°,120°	1.2	0.6173	2.36	0	4
2	30°, 120°	1.2, 1.5, 2.0, 3.0	0.6173	2.36	0	8
3	30°, 90°, 120°	1.2, 2.0	0.205, 0.4115, 0.6173, 0.823	2.36	0	24

3.3 Computational Domain

Bending sections in nature rivers are normally in irregular shapes, combined with the effect of wind which further complicates the issue. To establish a mathematical model and investigate the problem better, two assumptions are made: Firstly, the curved channels are extracted from part of circles; Secondly, winds are omitted. The computational domain (α=120°) with its boundary conditions and appropriate cross-section view are shown in Figure 1 as an example. The total length of the domain is $5L_{pp}$, in which the gravity of the ship model is situated in the middle. The distances between inlet and ship bow, outlet and stern are $2L_{pp}$ respectively. The slope angle of both bank sides is 27°, and the height of the domain is $5H$. The curved domain is ideally regarded as part of a circle and rotates around the circle center. The rotation rate is given to the meshes of the whole domain, inside which the ship is fixed, so there is no speed setting at the inlet. Besides, inlet and outlet are velocity inlet and pressure outlet; top is symmetry plane; channel bottom, concave side and convex side are all no-slip walls.

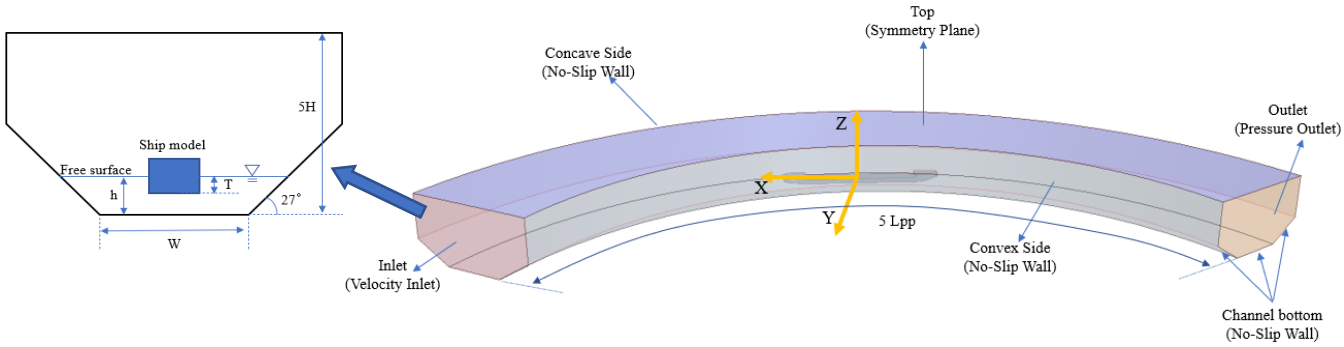

Figure 1. Computational domain(α=120°) with boundary conditions and its cross-section view

3.4 Mesh Sensitivity Analysis

Convergence study on the CFD model is focused on mesh sensitivity analysis. In this paper, resistance force, sway force and yaw moment are all expressed in non-dimensional forms according to equation (3):

$$X' = \frac{X}{\frac{1}{2}\rho V^2 L_{pp} T}, \quad Y' = \frac{Y}{\frac{1}{2}\rho V^2 L_{pp} T}, \quad N' = \frac{N}{\frac{1}{2}\rho V^2 L_{pp}{}^2 T} \tag{3}$$

The specific assessing procedures are conducted as reported by the guidelines of ITTC (28th ITTC, 2017). The configuration chosen is α=120°, h/T=1.2, V_S=0.6173m/s, W=2.36m, and β=0°, which are the relatively strict conditions in this study. Trimmed cell mesher and surface remesher are utilized to generate spatial and surface meshes. 6 prism layers with a growth factor of 1.5 are created to simulate the boundary layer. Additionally, grids are intensively processed in the free surface and the areas where the curvature of the hull surface changes a lot, such as the bow and the stern. The non-dimensional wall distance y^+ is lower than 1 for all simulations.

Three different grid sizes are imposed in the simulations with all the other conditions the same, and the

refinement ratio r_k is chosen as $\sqrt{2}$ according to the suggestion by ITTC. The mesh verification results are shown in Table 3. It can be seen that X' and Y' are both monotonic convergences, whereas N' belongs to oscillatory convergence. The mesh uncertainty of X', Y' and N' for all three grid settings are below 1%, which implies that the present simulations can predict results to an exact degree.

Table 3. Mesh convergence results

Grid	Grid number	X'	Y'	N'
Coarse	513302	0.1183067	0.0323387	-0.0549988
Medium	1521722	0.1118393	0.0110841	-0.0598951
Fine	5449767	0.110775	0.0095047	-0.0598819
R_i	—	0.1645626	0.0743094	-0.002683
Convergence condition	—	Monotonic	Monotonic	Oscillatory
C_i	—	5.076712338	12.4572308	—
δ_i	—	0.000209641	0.000126787	—
P_i	—	5.206581997	7.500619321	—
U_i	—	0.001918929	0.003032049	0.002448143

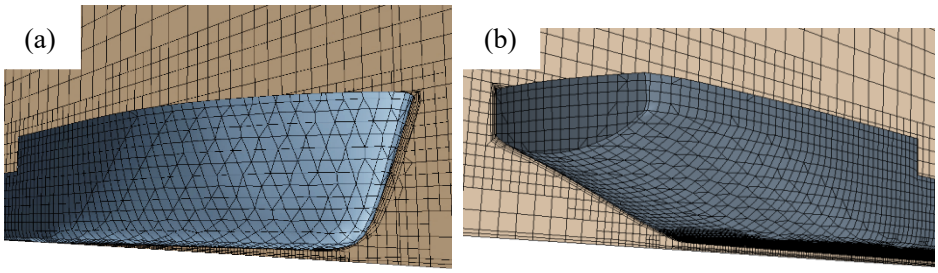

Figure 2. Mesh scene of the ship bow (a) and stern (b)

Considering the calculating efficiency, the medium grid displays a satisfying balance between calculating time and accuracy. Hence, the medium grid setting is used to carry out all the simulations. Mesh refinement near the ship is illustrated in Figure 2.

3.5 Validation of the Numerical Method

To validate the CFD model in this study, simulations of the ship maneuvering in a line channel (α=0°) are performed, where the optimal mesh is adopted. All the simulation settings are the same as those from the experiments that are supplied by CEREMA in France. The ship model is fixed in the fluid domain, and the speeds equaling required ship speeds are set to the inlet. Thus, resistance forces along *x* direction are compared with those from the experiments. Also, merely half ship is considered in the simulations to economize the computational time.

Table 4. Comparisons between simulations and experiments

Ship speed $V_s/m\ s^{-1}$	Resistance of numerical simulation X_n/N	Resistance of experiment (divided by 2) X_e/N	Errors E/%
0.335	0.690084	0.659	4.7%
0.4485	1.23664	1.194	3.5%
0.575	2.15804	2.124	1.6%

From Table 4, all the errors between simulations and experiments are within 5% for different V_s, so a good agreement can be assumed between the CFD results and experimental data. It's practicable to investigate the current research with this CFD model.

4. Result and Discussion

The simulation results based on the configuration settings in Table 2 are displayed and analyzed in detail. Resistance force(X), sway force(Y)and yaw moment(N) of the ship are transformed into non-dimensional forms which are expressed as X', Y' and N' respectively. Also, the positive directions for X and Y are assumed opposite to x and y coordinate axis, and the positive direction for N is counter-clockwise on paper. Meanwhile, the hydrodynamic forces and moment are broken up into pressure component and frictional component due to $X' = X'_p + X'_f$, $Y' = Y'_p + Y'_f$, $N' = N'_p + N'_f$, where prime 'p' and 'f' indicate pressure and friction respectively.

4.1 Effect of channel angle (α) on ship hydrodynamics

This section analyzes the impact of α on ship hydrodynamics, in which the results are based on the simulations of Config.1 in Table 2. A common consensus should be pointed out that the larger α is, the larger the curvature of a channel is under the condition of the same channel length. According to Figure 3, X' increases a little as α grows. While a slight decrease in X'_p and increase in X'_f can be observed respectively, and meanwhile X'_p is always nearly twice as large as X'_f. It can be noticed in Figure 4 that waves generated around the convex bank are disappearing with α growing, and there are only waves around the concave bank under large α. This contributes to the increase of X'_p. Combined with the streamlines in Figure 5, it can be seen that the curvature of the mainstream is becoming larger as α grows, and streams come nearer the concave bank when passing through the ship. In this way, the flow area further diminishes as α grows, which causes a difference in water depth between convex and concave banks. Then the flow velocity around the ship will increases due to the Venturi effect, resulting in an increase in X'_f.

Y' increases by a relatively large margin as α grows for α<60°(increasing rate 44.39%). However, Y' starts diminishing after α exceeds the critical value 60°, and especially declines fast for α>90°(decreasing rate 75%). It should be noted that Y' grows again with its direction changing from pointing towards the concave bank to pointing towards the convex bank for α>115°, which is under the influence of the large channel curvature. To verify this somewhat complex tendency of the curve, another two configurations(α=75° and α=105°) are added, and their results coincide with this trend. According to Figure 4, wave reflections on convex bank sides are disappearing as α grows. From the discussion above, the mainstream flows near the concave bank under large α. This intensifies the interaction between the ship and the concave bank in channels of large α, and consequently, the ship is subjected to Y' pointing towards the convex bank (the positive direction of Y' is towards the concave bank).

N' poses a rapid growing tendency as α grows. Also, the pressure components dominate in Y' and N' with appropriate frictional components around 0 due to the bow and stern effect. Thus, drift caused by N' can easily occur with α increasing. Worse still, a large number of sediments and suspensions exist in actual rivers, and these sediments will accumulate around the concave bank caused by the spiral flow. This spiral flow is the combination of loop flow and longitudinal flow, which is also the flow of mainstreams in bending rivers. As a result, the water depth here will become smaller than the other parts of the river. The ship is consequently more likely to go aground if it maneuvers near the concave bank due to drift while passing the bending section.

Special attention should be paid when a ship is advancing in channels with large α, and frequent rudder angle control can be taken to reduce yaw.

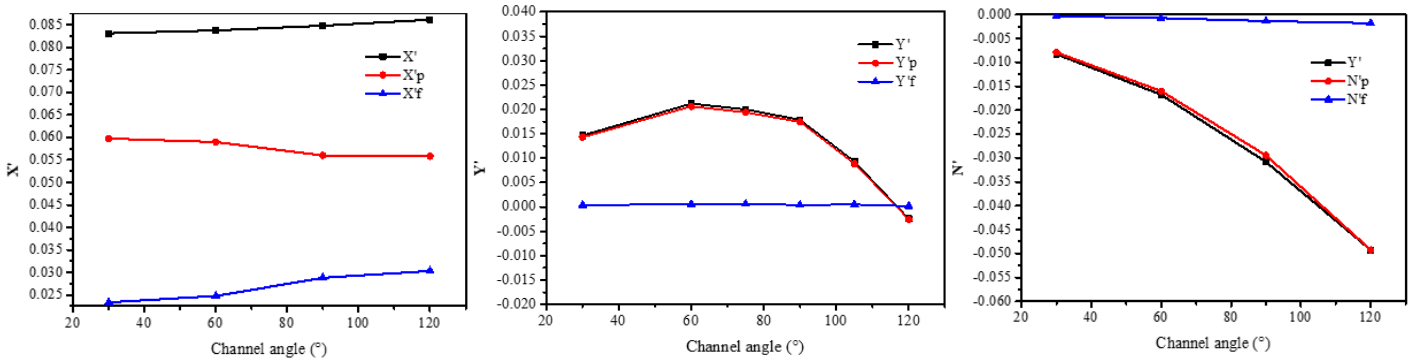

Figure 3. Non-dimensional hydrodynamic forces and moment with pressure and frictional components under different α

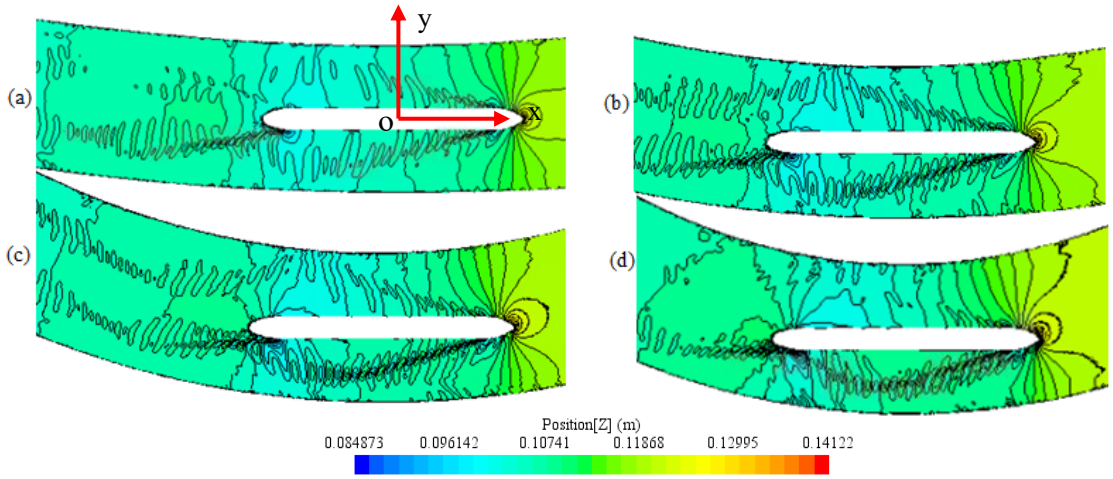

Figure 4. Wave elevation contours for Config.1
(a) to (d): α=30°, 60°, 90°, 120°

As is also depicted in Figure 5, the pressure along the hull is increasing with α enlarging, which is in agreement with the increase in wave elevation with α growing(See Figure 4). This is caused by the uneven distribution of water depth and the much stronger spiral flow in the channel of large α. However, the high-pressure parts are concentrated around the ship bow for all α values in this study, and this signifies the increasing tendency of trim by stern with the increment of α.

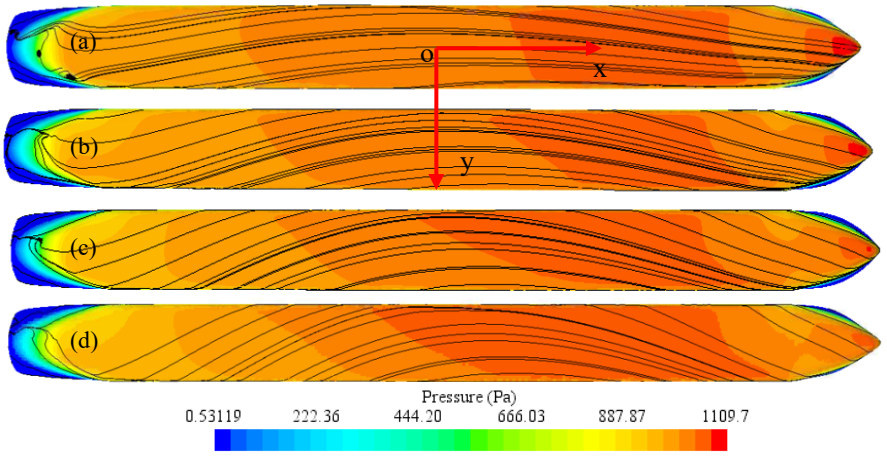

Figure 5. Pressure distribution with streamlines along the ship hull for Config.1 (a) to (d): α=30°, 60°, 90°, 120°

4.2 Effect of *h/T* ratio on ship hydrodynamics

Section 4.2 elaborates the effect of *h/T* on ship hydrodynamics, whose consequences come from the simulations of Config.2 in Table 2. In this paper, it's defined: *h/T*=1.2 confined waters, *h/T*=1.5 shallow waters, *h/T*=2.0 medium-deep waters, *h/T*=3.0 deep waters.

As is shown in Figure 6, X' decreases rapidly for both α=30° and α=120° with *h/T* increasing, especially in shallow waters. Whereas for *h/T*>2(deep waters), the decreasing trend slows down for channels of both α. At the same time, there is not much difference in X' between the two curves of large and small α as function of *h/T*. Given that the two configurations (α=30° and α=120°) share a similar pattern of change in component variations, the component variation for α=30° is taken as example in Figure 7, where X'_p is also decreasing as *h/T* grows with X'_f hardly changing. When *h/T* is above 1.9 or so, X'_p is lower than X'_f.

A relatively large decline in Y'(decreasing rate 88.06%) in the channel of α=30° can be observed for *h/T* <1.5(shallow waters), which declares the high sensitivity of Y' to *h/T* in shallow waters of the small-curvature channel. After *h/T* exceeds 1.5, Y' decreases little. While no large change can be noticed in the channel α=120°, which shows the influence of *h/T* is insensitive in the large-curvature channel. The direction of Y' is also opposite for channels with large (α=120°) and small (α=30°) α, and Y' for α=120° is normally slightly larger than that for α=30° apart from in the confined waters (*h/T*<1.5).

For both α=120° and α=30°, N' decreases faster in shallow waters compared with that in deep waters as *h/T* increases. N' in the channel of α=120° diminishes fast, especially a reducing rate of 52% can be observed for *h/T*< 1.5(shallow waters) as *h/T* grows. While N' in the channel of α=30° doesn't change much, except for the slightly noticeable variation for *h/T*< 1.5. Also, Y'_p and N'_p dominate in Y' and N' with their respective frictional components approaching 0, which is due to the bow and stern effect (see Figure 7).

The pressure around the ship is decreasing with *h/T* growing regardless of α. Under the same *h/T* ratio, the pressure distributed around the ship for α=120° is always higher than that for α=30°. Most importantly, pressure distribution around the ship in curved channels is different from our previous knowledge about the shallow water effect. In curved channels, pressure around the ship is increasing as *h/T* reduces.

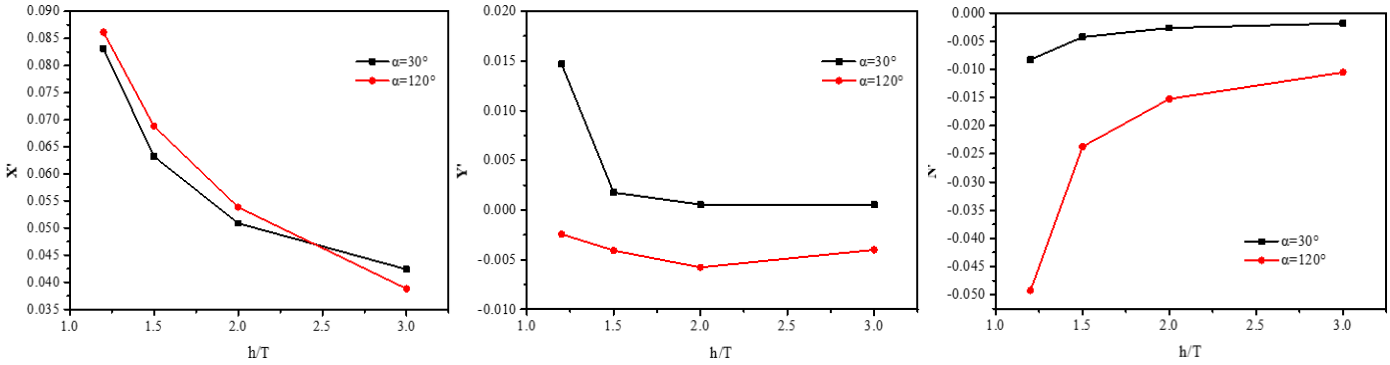

Figure 6. Non-dimensional hydrodynamic forces and moment of the ship under different *h/T* ratios

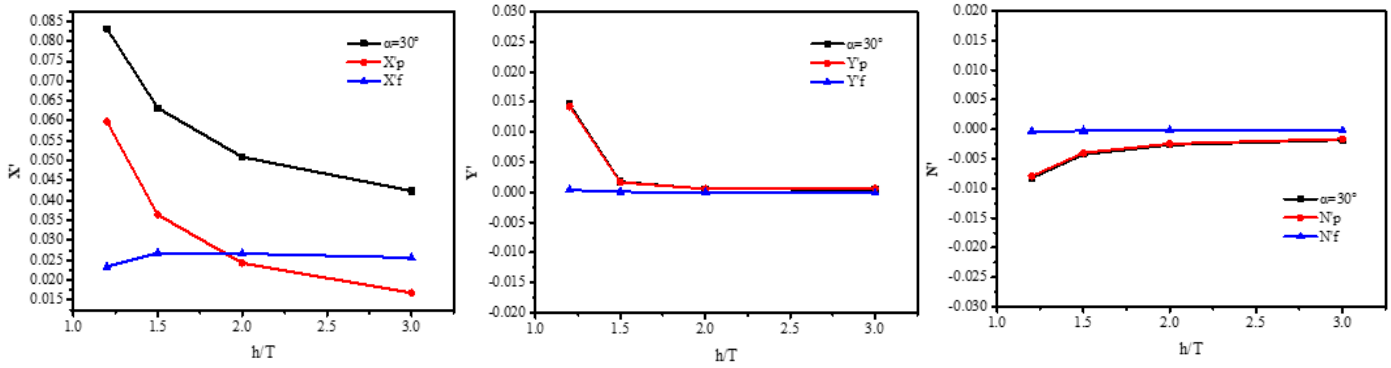

Figure 7. Pressure and frictional components for α=30° in Config.2

4.3 Effect of ship speed(V_s) on ship hydrodynamics

Section 4.3 is dedicated to explaining the influence of V_s on ship hydrodynamics, where the results are based on Config.3 in Table 2.

According to Figure 8, there is not much difference in X' at low V_s for all configurations. As V_s increases, X' is increasing faster and faster for all configurations. However, X' in confined waters(*h/T*=1.2) is always growing more rapidly than that in medium-deep waters(*h/T*=2.0), which means X' in shallow waters tends to be more sensitive to V_s than that in deep waters. Based on the conclusion from Section 4.1, α poses little effect on X'. This is proved again here, and we can go further and conclude that V_s almost does not affect X' under different α. Whereas under different V_s, only *h/T* influences X' much. The configuration α=120° *h/T*=2 is taken as example in Figure 9 to show the force and moment components. X'_p and X'_f occupy nearly the same proportion in X'.

As for Y', abnormal descending trends appear for the two configurations of α=120°. To verify the tendencies, two simulations of V_s=0.72m/s and V_s=0.8m/s are added to the configuration α=120°, *h/T*=1.2. Also, one simulation of V_s=0.72m/s is added to the configuration α=120°, *h/T*=2. Their results follow the trends of the two curves, which confirms the correctness of the curve tendencies. For α=30° and α=90°, Y' in confined waters(*h/T*=1.2) is increasing faster as V_s grows, while Y' in medium-deep waters (*h/T*=2.0) nearly keeps constant. However, for α=120°, Y' decreases very little for both deep and confined waters when V_s is lower than a critical value. The critical value for shallow waters is around 0.72m/s, and is about 0.4115m/s for deep waters. The opposite direction of Y' in this configuration compared with the others has been proved in Section 4.1. When V_s exceeds the critical value, Y' starts increasing a lot as V_s grows, and the magnitude of increase in confined waters(*h/T*=1.2) is even more dramatic than that in medium-deep waters(*h/T*=2). The reason is that wave-making around the ship is serious enough at a high V_s. Consequently, reflected waves

counteracted by the concave bank will be returned to act on the ship hull. This interaction gives the hull a force in the same direction of Y', which intensifies Y'.

As V_s grows, N' is increasing for all the configurations here. However, it's obvious that N' enlarges fast in the channel with larger α and in shallower waters. Only in the channel with large α(α=90° and 120°), h/T ratio influences N' obviously at different V_s. The pressure components dominate in both Y' and N'(see Figure 9). Hence, it's significant for a ship to advance at a low V_s in order to minimize or avoid the effect of spiral flow in curved channels on ship maneuverability.

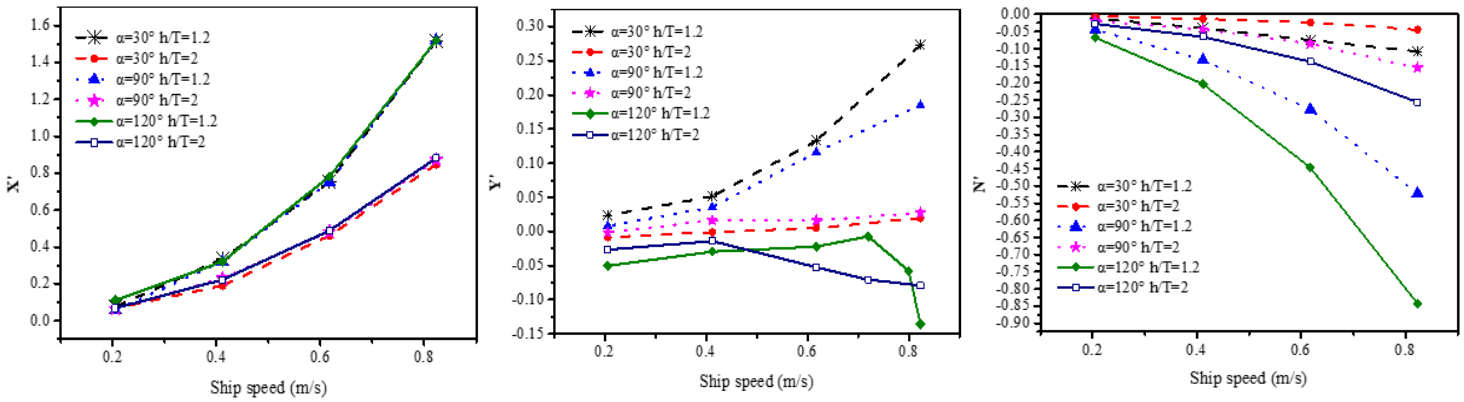

Figure 8. Non-dimensional hydrodynamic forces and moment of the ship under different V_s

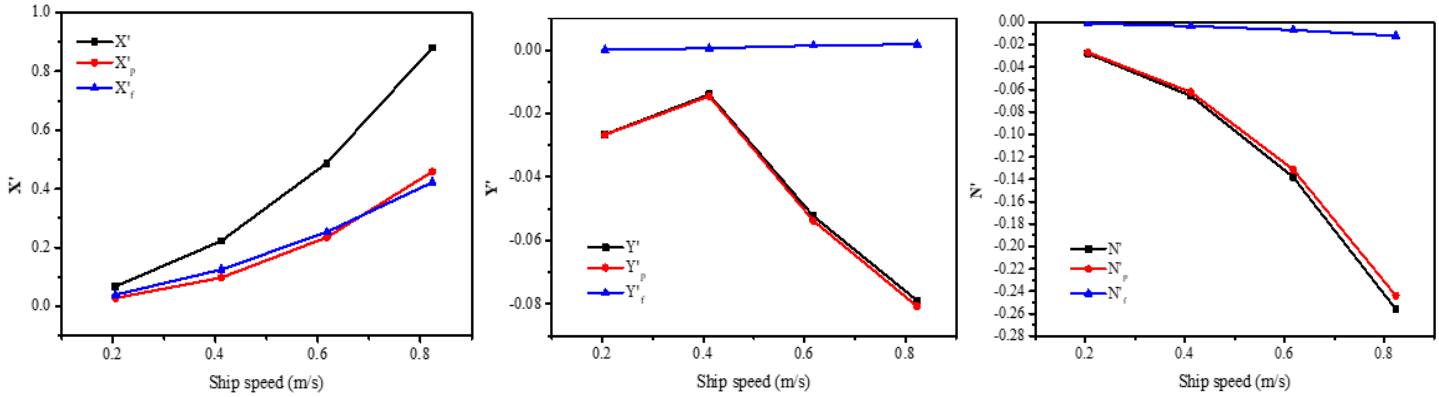

Figure 9. Pressure and frictional components for α=120° h/T=2 in Config.3

5. CONCLUSIONS

In this paper, unsteady RANS simulations based on K-ϵ turbulence model were conducted to investigate the characteristics of confined curved channels on hydrodynamic forces and moment of the inland ship. To ensure an effective CFD model for this study, a mesh convergence analysis was performed to select the most proper grid setting. Meanwhile, a validation test was carried out to prove that the numerical simulation can predict hydrodynamic results accurately. A series of vital parameters for ship's navigation in curved fairways including channel angle, h/T ratio, and ship speed were chosen to investigate the impact of these parameters on X, Y, N respectively. The consequences are analyzed as follows:

(1) As α increases, X' of the ship grows very little. There exist a critical value of α for Y', and a fast downward trend of Y' can be observed after α exceeds this value. While N' grows at a rapid rate as α grows, which easily causes the ship to yaw. X'_p nearly accounts for 2/3 of $X'$with X'_f occupying 1/3, whereas

Y'_p and N'_p dominate in Y' and N' respectively.

The elevated pressure distributed around the hull can also be observed with α increasing due to the larger curvature of streamlines, especially for pressure at bow. Thus, the increasing tendency of trim by stern can be assumed in a channel of larger α. Besides, the interaction between the ship and the concave bank is more serious for larger α, while it's much weaker with the convex bank.

(2) X' is very sensitive to *h/T* ratio regardless of α, and X' decreases fast with *h/T* increasing. While the effect of *h/T* on Y' is small, and an obvious downward tendency in Y' can be only observed for small-curvature channels(α=30°) in shallow waters(*h/T*<1.5). N' is sensitive to both *h/T* and α. For α=120°, N' diminishes fast in shallow waters as *h/T* increases, but its magnitude of change becomes small when *h/T* exceeds 2. For α=30°, N' goes down slowly with *h/T* increasing in shallow waters, while it's almost unchanged after that. Besides, X'_p dominates in shallow waters, but X'_f starts coming to dominance after *h/T* surpasses a critical value. Yet Y'_p and N'_p dominate all the time. Hence, an increase in water depth is beneficial for eliminating the resistance and yaw of a ship.

However, pressure around the ship will increase with *h/T* ratio reducing. This is different from what we know about the shallow water effect.

(3) X' increases faster and faster with V_s growing, especially in shallow waters. For α≤90° in shallow waters(*h/T*=1.2), Y' is increasing more and more with V_s ascending; For α≤90° in deep waters(*h/T*=2), Y' increases little with V_s growing. While for α=120°, Y' starts rising a little as V_s grows. But when V_s exceeds a critical value, Y' commences reducing due to the strong interaction with the concave bank. Moreover, the critical V_s for shallow waters is larger than deep waters, and Y' declines more seriously in shallow waters after the critical V_s. N' is increasing for all the configurations as V_s rises, but N' boosts faster for larger α and shallower waters. Specifically, *h/T* affects N' more for large α, while α influences N' more for shallow waters. Also, X'_p and X'_f occupy nearly the same proportion in X', while pressure components dominate in Y' and N'.

(4) Allowing for the page limit, we didn't present two points here. One is the effect of channel bottom width(*W*) and drift angle(β) on ship hydrodynamics, and the other is maneuvering analysis. They will be shown in the future. Also, this is the first work to understand what the flow behaviors are around the ship in confined curved channels, regarding different parameters such as channel angle(α), *h/T* ratio, ship speed(V_s). The following work is to find mathematical formulations to be included in the simulators, aiming at taking account of these effects. In this way, the behaviors of ships in the sensitive regions can be corrected.

ACKNOWLEDGEMENTS

The research in this paper was funded by China Scholarship Council (CSC), and Center for Studies and Expertise on Risks, the Environment, Mobility and Urban Planning (CEREMA-DtecREM) in France.

REFERENCES

Aseperi, O., 2018. Dynamics of Flow in River Bends. Colorado State University.

Bechthold, J., Kastens, M., 2020. Robustness and Quality of Squat Predictions in Extreme Shallow Water

Conditions Based on RANS-calculations. Ocean Engineering 197.

Elsherbiny, K., Terziev, M., Tezdogan, T., Incecik, A., Kotb, M., 2020. Numerical and Experimental Study on Hydrodynamic Performance of Ships Advancing Through Different Canals. Ocean Engineering 195.

Kaidi, S., Lefrançois, E., Smaoui, H., 2020. Numerical Modelling of the Muddy Layer Effect on Ship's resistance and Squat. Ocean Engineering 199.

Kaidi, S., Smaoui, H., Sergent, P., 2018. CFD Investigation of Mutual Interaction between Hull, Propellers, and Rudders for an Inland Container Ship in Deep, Very Deep, Shallow, and Very Shallow Waters. Journal of Waterway, Port, Coastal, and Ocean Engineering 144 (6).

Kaidi, S., Smaoui, H., Sergent, P., 2017. Numerical Estimation of Bank-propeller-hull Interaction Effect on Ship Manoeuvring Using CFD Method. Journal of Hydrodynamics 29 (1), 154-167.

Li, H., Dong, H., Ji, P., 2020. Curved Water Flow Characteristics and Its Influence on Navigation. Vibroengineering Procedia 33, 102-106.

Razgallah, I., Kaidi, S., Smaoui, H., Sergent, P., 2018. The Impact of Free Surface Modelling on Hydrodynamic Forces for Ship Navigating in Inland Waterways: Water Depth, Drift Angle, and Ship Speed Effect. Journal of Marine Science and Technology 24 (2), 620-641.

Srđan Vujičić, Robert Mohović, Tomaš, I.Đ., 2018. Methodology for Controlling the Ship’s Path during the Turn in Confined Waterways. Scientific Journal of Maritime Research.

Terziev, M., Tezdogan, T., Oguz, E., Gourlay, T., Demirel, Y.K., Incecik, A., 2018. Numerical Investigation of the Behaviour and Performance of Ships Advancing Through Restricted Shallow Waters. Journal of Fluids and Structures 76, 185-215.

Tezdogan, T., Incecik, A., Turan, O., 2015. A Numerical Investigation of the Squat and Resistance of Ships Advancing Through A Canal Using CFD. Journal of Marine Science and Technology 21 (1), 86-101.

Tezdogan, T., Incecik, A., Turan, O., 2016. Full-scale Unsteady RANS Simulations of Vertical Ship Motions in Shallow Water. Ocean Engineering 123, 131-145.

Wanzheng Ai, Zhu, P., 2020. Navigation Ship’s Drift Angle Determination Method in Curved Channel. Journal of Coastal Research.

28th ITTC, 2017. Uncertainty Analysis in CFD Verification and Validation Methodology and Procedures. ITTC – Recommended Procedures and Guidelines 7.5-03 -01-01 Page 1 of 13.